Supporting Information

for

Near-field infrared nanospectroscopy reveals guest confinement in metal-organic framework single crystals

Annika F. Möslein[a], Mario Gutiérrez[a], Boiko Cohen[b] and Jin-Chong Tan[a]*

[a]Multifunctional Materials & Composites (MMC) Laboratory, Department of Engineering Science, University of Oxford, Parks Road, Oxford OX1 3PJ, United Kingdom.

[b]Departamento de Química Física, Facultad de Ciencias Ambientales y Bioquímica, and INAMOL, Universidad de Castilla-La Mancha, Avenida Carlos III, S.N., 45071 Toledo, Spain.

*jin-chong.tan@eng.ox.ac.uk

Contents

1 METHODS

1.1 SYNTHESIS PROTOCOLS

1.1.1 Synthesis of ZIF-8

Nanocrystals of ZIF-8 [Zn(mIM)$_2$; mIM = 2-methylimidazolate] were synthesised by dissolving 4.5 mmol of zinc nitrate hexahydrate ($Zn(NO_3)_2 \cdot 6H_2O$, 98%, Sigma-Aldrich) and 13.5 mmol 2-methylimidazole (98%, Sigma-Aldrich) in 60 mL of methanol, respectively. After combining the two clear solutions, the white colloidal solution was rigorously stirred for 1 min and then left to form the nanocrystals. After 60 min, nanocrystals were isolated by centrifugation at 8000 rpm for 10 min and, subsequently, the clear solution was substituted with fresh methanol. To remove any excess or unreacted metal salts and/or organic linkers, this washing process was repeated three times. Subsequently, the samples were drop casted onto gold substrates and dried at 80 °C for 4 hours in vacuum to remove any residual methanol as preparation for AFM characterisation.

1.1.2 Synthesis of RhB@ZIF-8

3 mmol of $Zn(NO_3)_2 \cdot 6H_2O$ was diluted in 20 mL of dimethylformamide (DMF). Similarly, 7.5 mmol of 2-methylimidazole was dissolved in 20 mL of DMF with addition of 7.5 mmol of triethylamine. The linker and the dye solution, the latter formed by 0.05 mmol (24 mg) of rhodamine B in 10 mL DMF, were mixed and later added to the metal ion solution. The material obtained was washed with 50 mL of fresh DMF, followed by two washing steps with acetone (termed RhB@ZIF-8 as synthesised). For additional, thorough washing, the material was diluted in 30 mL of fresh methanol under constant stirring for 60 min before centrifugation at 8000 rpm for 10 min to isolate the crystals. Subsequently, the same procedure was followed with fresh acetone. Both steps were alternated 5 times. Finally, the isolated nanocrystals were dried at 80 °C for 4 hours in vacuum.

1.1.3 Synthesis of UiO-66

Single crystals of UiO-66 [$Zr_6O_4(OH)_4(BDC)_6$; BDC = benzene-1,4-dicarboxylate] were prepared following a previously reported method.[1] Briefly, 0.4 mmol (93 mg) of zirconium chloride anhydrous ($ZrCl_4$, Fisher Scientific) and 0.4 mmol (67 mg, Fisher Scientific) of terephthalic acid were independently dissolved in 10 mL of DMF each. Then, 50 mmol (2.8 mL, Fisher Scientific) of glacial acetic acid were poured into the terephthalic acid solution and this mixture was transferred to a Pyrex bottle containing the $ZrCl_4$ solution. The final mixture was heated in an oven at 120 °C for 24 h. The white solid powder was thoroughly washed with DMF and MeOH, collected by centrifugation (8000 rpm), and dried at 120°C under vacuum overnight.

1.1.4 Synthesis of RhB@UiO-66 and fluorescein@UiO-66

The guest@UiO-66 materials were synthesised similarly to the UiO-66 crystals but involving one additional step. On one side, 0.4 mmol (93 mg) of $ZrCl_4$ were dissolved in 10 mL of DMF. On the other side, 0.4 mmol (67 mg) of terephthalic acid, 3 mg of the guest dye (RhB or fluorescein) and 2.8 mL of glacial acetic acid were added to 10 mL of DMF. Both solutions were mixed into a Pyrex bottle, and the mixture was heated in an oven at 120 °C for 24 h. The yellow (fluorescein) and pink (RhB) powder samples were thoroughly washed with DMF and MeOH until two consecutive supernatants were transparent and non-emissive under UV irradiation (this typically involves between 5-7 washing steps). After that, the powder samples were collected by centrifugation (8000 rpm), and dried at 90 °C under vacuum overnight.

1.2 MATERIALS CHARACTERISATION

1.2.1 PXRD and FTIR

Powder X-ray diffraction (PXRD) and FTIR confirmed the successful synthesis of ZIF-8 and UiO-66. PXRD patterns were measured using the Rigaku MiniFlex diffractometer equipped with a Cu Kα source (step size of 0.02° and 0.01°/min) and validated against the simulated XRD pattern. Attenuated total reflection (ATR)-FTIR measurements on the (bulk) polycrystalline powder material were performed using the Nicolet iS10 FTIR spectrometer. Scanning electron microscope (SEM) images of the samples were obtained with a TESCAN LYRA3 electron microscope.

1.2.2 NanoFTIR Measurements

The near-field optical measurements were performed using the neaSNOM instrument (neaspec GmbH) based on a tapping-mode AFM where the platinum-coated tip (NanoAndMore GmbH, cantilever resonance frequency 250 kHz, nominal tip radius ~20 nm) was illuminated by a broadband infrared (IR) laser. The coherent mid-infrared (MIR) light (700-2400 cm^{-1}) was generated through the nonlinear difference-frequency combination of two beams from fibre lasers (TOPTICA Photonics Inc.) in a GaSe crystal. By demodulating the optical signal at higher harmonics of the tip resonance frequency and employing a pseudo-heterodyne interferometric detection module, amplitude and phase of the scattered wave from the tip are measured, hence, yielding the complex optical response of the material without background signals.[2] We probed individual MOF crystals by averaging over three measurements with 20 individual point spectra each. At least 20 different crystals or regions were probed for each sample. Each spectrum was acquired from an average of 20 Fourier-processed interferograms with 10 cm^{-1} spectral resolution, 2048 points per interferogram, and an 18-ms integration time. The sample spectrum was normalised to a reference spectrum measured on a gold surface to reconstruct the final nanoFTIR amplitude and phase. The continuous broadband MIR spectra were attained by combining two illumination sources, then the obtained spectra were joined at 1500 cm^{-1}. All measurements were carried out under ambient conditions (~40% RH).

1.2.3 s-SNOM Imaging

The s-SNOM contrast images were measured at neaspec GmbH (Haar, Germany). As the source of monochromatic irradiation, a tuneable quantum cascade laser (Daylight solutions) was employed with output powers tuned to approximately 2 mW. For each scan, the pixel integration time was set as 16 ms. The tip was operating at a frequency of 253 kHz. The recorded signal was demodulated at the third harmonic through a pseudo-heterodyne detection mode. It is worth mentioning that the measurements were repeated at various positions for a systematic characterisation of the sample, and only exemplary scans are presented in Figures 3 & 5 of the main manuscript.

1.2.4 Fluorescence Spectroscopy

Steady-state fluorescence spectra were recorded employing the FS-5 spectrofluorometer (Edinburgh Instruments) equipped with different modules for specific measurements. For RhB@ZIF-8, the powder samples were dispersed in acetone, and the SC-05 module, a standard cuvette holder for liquid samples, was used. Excitation and emission spectra of UiO-66 and Guest@UiO-66 powder samples were obtained using the SC-10 module for solid materials. The detection and excitation wavelengths for measuring the steady-state excitation and emission spectra, respectively, are indicated in the corresponding figures. Each measurement is acquired from two scans with a dwell time of 0.2 s and a step size of 1 nm.

1.2.5 Fluorescence Lifetime Imaging Microscopy (FLIM)

The encapsulation of fluorescein into UiO-66 was further corroborated by using a confocal fluorescence microscope. Fluorescence lifetime images (FLIM) of fluorescein@UiO-66 were recorded using an inverted-type scanning confocal fluorescence microscope (MicroTime-200, Picoquant, Berlin) with a 60× NA1.2 Olympus water immersion objective, and a 2D piezo scanner (Physik Instrumente). A 470-nm pulsed diode laser (pulse width ~40 ps) was employed as the excitation source. A dichroic mirror (AHF, Z375RDC), a 500-nm long-pass filter (AHF, HQ500lp), a 75-μm pinhole, and an avalanche photodiode detector (MPD, PDM series) were used to collect the emission. The emission spectrum was recorded using a spectrograph (Andor SR 303i-B) equipped with a 1600 × 200 pixel EMCCD detector (Andor Newton DU-970N-BV) coupled to the Micro-Time-200 system.

Note that only the fluorescein@UiO-66 crystals can be probed under this FLIM system using the available excitation source of 470 nm. Unfortunately, RhB cannot be studied by the current setup because this will require an excitation source of at least 520 nm.

1.2.6 Density Functional Theory (DFT) Calculations

The theoretical vibrational spectrum of ZIF-8 was computed using DFT at the PBE level of theory[3] with a damped empirical dispersion term (PBE-D).[4] The calculations were carried out with the periodic *ab initio* CRYSTAL14 code.[5] After a geometry optimisation, the Berry Phase approach[6] was employed to compute the IR intensities. A continuous spectrum was obtained by fitting the calculated IR intensities with Lorentzian peak shapes with a FWHM of 10 cm^{-1}.

DFT calculations to determine the theoretical vibrational spectrum of RhB were performed using GAUSSIAN 09 software.[7] Both the geometry optimisation and final frequency calculations were carried out by employing the BLYP/6-311+G(2d,p) basis set.

2 FURTHER DETAILS: MEASURING THE LOCAL INFRARED ABSORPTION SPECTRA

The processed s-SNOM data yield the optical properties of the sample at a nanoscale (henceforth we refer to such properties as 'local'). Derived from the standard theoretical description of s-SNOM, the scattering coefficient relates the incident field with the scattered field from the tip. Since the backscattered light from the tip is modified by the near-field interaction with the sample, the complex-valued scattering coefficient contains information about the sample permittivity. However, the signal is dominated by the background scattering. To extract the near-field interaction, the detector signal is modulated at higher harmonics of the tapping amplitude of the AFM tip. Demodulation of the interferometric detector signal is achieved by a complex Fourier transform with respect to time. Here, it is worth mentioning that the model for the scattering coefficient includes the tip height above the sample surface, which depends on time due to the oscillation of the tip.

The Fourier transformation yields the sample dielectric function, from which the local permittivity can be extracted, for a detailed mathematical description we refer to Govyadinov *et al.*[8] Note that the measured data includes contributions from the setup, hence normalisation to a reference signal is required. This provides the complex-valued near-field contrast with its corresponding amplitude and phase. However, the imaginary part of the near-field contrast obtained through nanoFTIR depicts a better match with the far-field FTIR absorption spectra,[8] where the absorption coefficient is attained *via* the Kramer's-Kronig relations.[9] Therefore, the nanoFTIR absorption is defined as the imaginary part of the near-field contrast.

Hence, only the imaginary part is shown in this work. For completeness, Figure S1 summarises the raw data of the amplitude, phase, as well as the real and imaginary parts measured on an individual ZIF-8 crystal, and normalised to the gold substrate. The continuous broadband MIR spectrum is attained by combining two illumination sources. First, Laser 1 (700 – 1400 cm^{1}) was employed to measure the reference spectra on the clean gold substrate, acquired from an average of 20 interferograms. Each interferogram was measured with a 10 cm^{-1} spectral resolution, 2048 points per interferogram and with an 18-ms integration time.

Secondly, the ZIF-8 crystal, for instance, was probed to attain the nanoFTIR spectra, which were divided by the reference spectra. To reduce the noise, three measurements on the same location of the crystal were performed and averaged. The same procedure was repeated after switching the IR illumination source to Laser 2 (1250 – 2100 cm^{-1}). As shown in Figure S1, the spectra obtained from the same crystal matched well in the overlapping region and can thus be combined to yield the broadband spectra from 700 to 2100 cm^{-1}.

Figure S2 depicts exemplary positions, where the local nanoFTIR spectra were measured. To examine the IR spectra from the MOF materials, at least 20 individual crystals were measured and compared to obtain information about the local chemical variability of the individual crystals as well as to determine the properties of the sample, when averaged over the measurements on several single crystals.

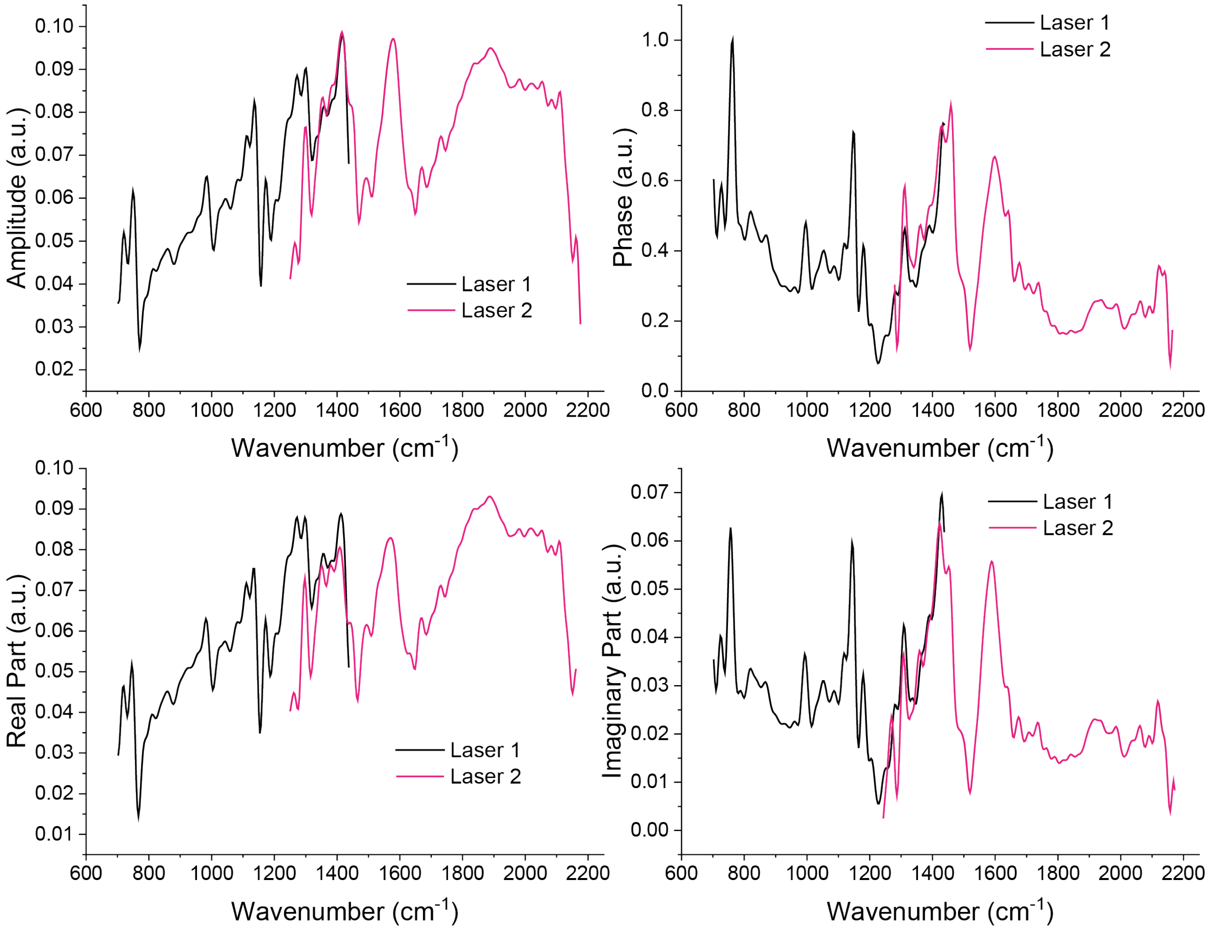

Figure S1: Amplitude, phase, real and imaginary parts of the near-field spectra obtained through nanoFTIR measurements on a single crystal of ZIF-8, normalised to a gold substrate.

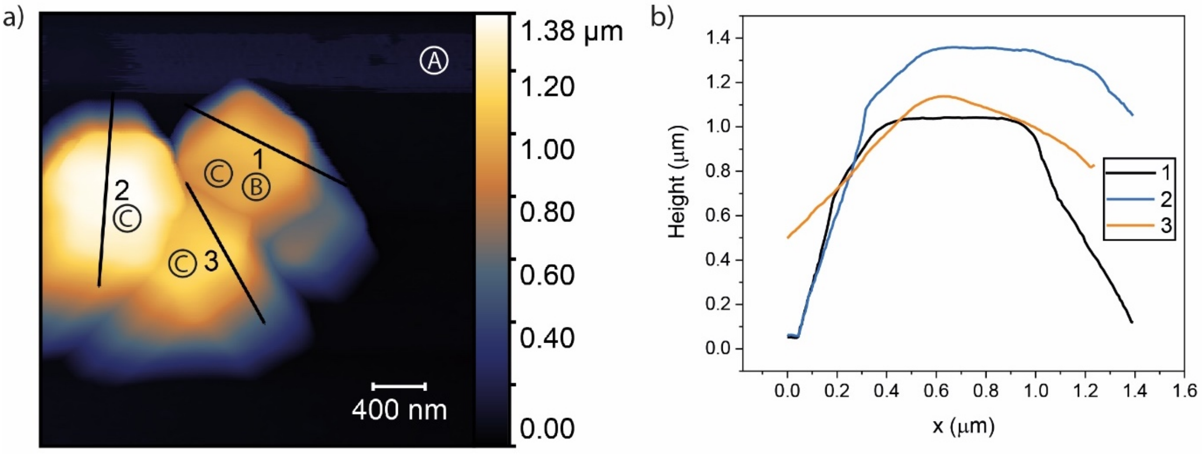

Figure S2: a) The exemplary positions of the local nanoFTIR measurements performed on micron-sized crystals. Region A: reference spectrum measured on silicon or gold substrate. Region B: Three measurements with 20 individual point spectra each were performed to obtain the local properties of an individual crystal. Regions C: Several crystals were measured (at various positions on the sample, not shown here) and further compared to probe the sample-specific properties. b) Height profiles of the crystals along the designated lines (1-3) in the AFM image.

3.1 X-RAY DIFFRACTION (XRD)

XRD was employed to confirm the crystalline structure of the powder samples. Through comparison of the experimental measurements with simulated reference patterns, the successful synthesis of the MOF crystals was validated as shown in Figures S3 & S4. The crystal structure of the RhB@ZIF-8 system is in agreement with the simulated ZIF-8 pattern. Figure S4 reveals the intact crystalline structure of the guest@UiO-66 systems (guest = rhodamine B or fluorescein), matching the diffraction pattern of the pristine UiO-66 crystal. The reference XRD patterns were analysed using the CrystalDiffract software, using CIF files from the Cambridge Structural Database (CSD) database as input.

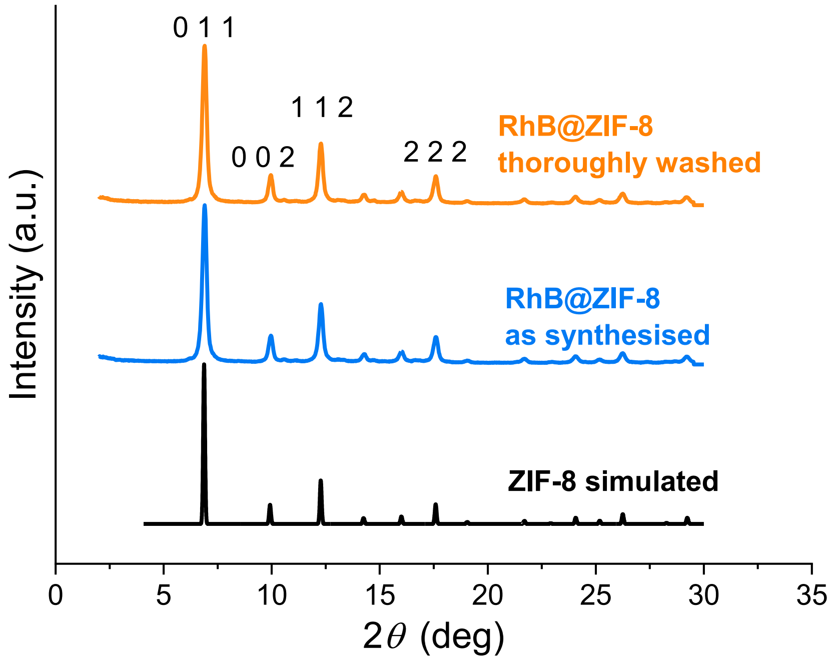

Figure S3: XRD patterns of RhB@ZIF-8 powder samples compared with the simulated pattern of ZIF-8.

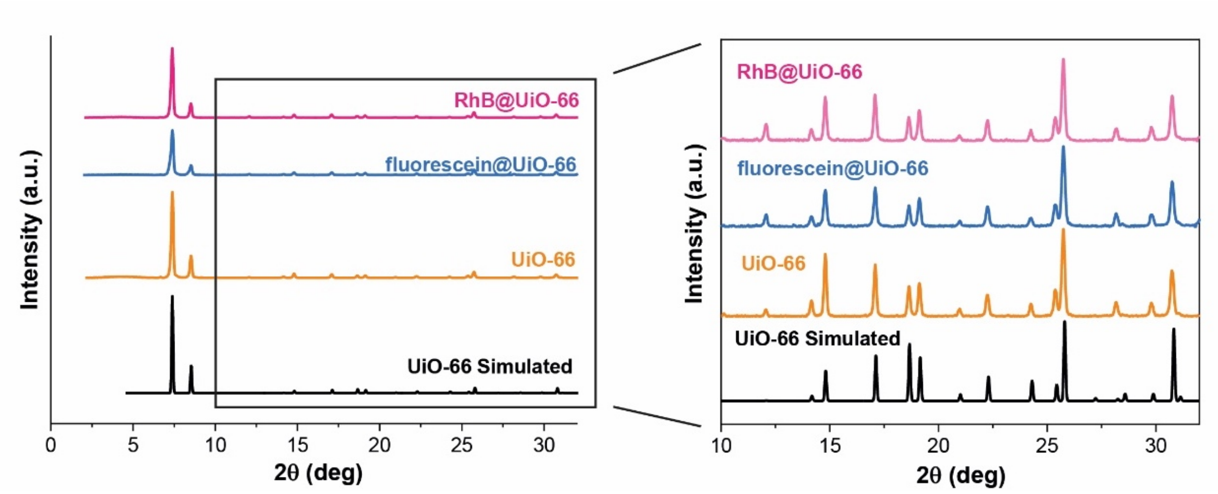

Figure S4: XRD patterns of the guest@UiO-66 composite systems.

3.2 ATOMIC FORCE MICROSCOPY (AFM)

AFM yields a topographical image of a sample surface at nanometre resolution. In addition, the roughness of a surface or the thickness of a crystal can be quantified. AFM imaging was performed with a neaSNOM instrument (neaspec GmbH) operating in tapping mode. Height topography images were collected using the Scout350 probe (NuNano), which has a nominal tip radius of 5 nm, a spring constant of 42 N/m and resonant frequency of 350 kHz. Figures S5 – S7 exemplarily demonstrate height profiles of the MOF crystals under investigation. Further, the AFM measurements were combined with nanoFTIR spectroscopic data to yield the combined topographical and chemical information at the nanoscale.

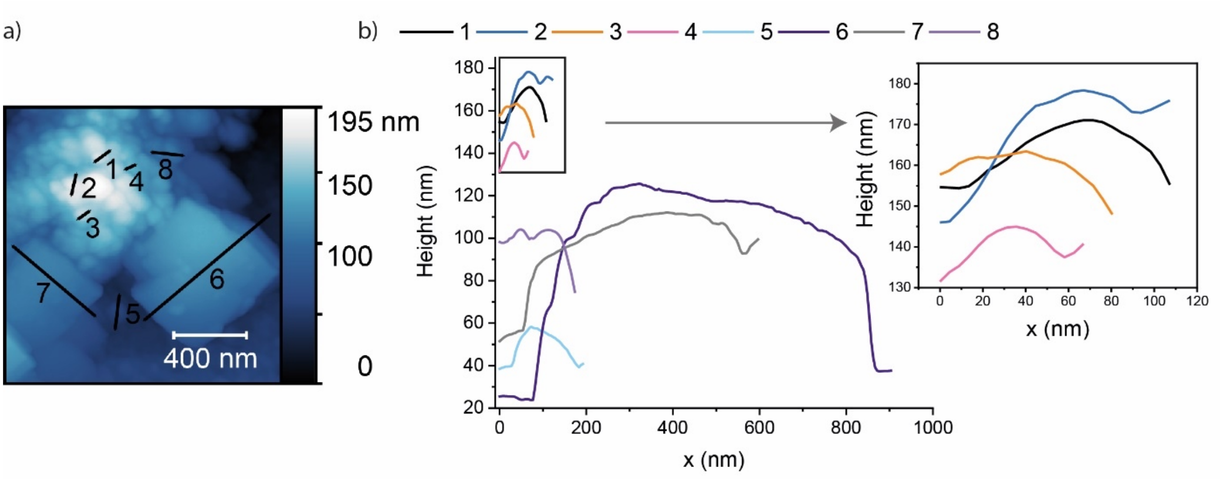

Figure S5: (a) AFM image of the ZIF-8 nanocrystals and RhB blocks. (b) Surface height profiles corresponding to the designated lines in (a).

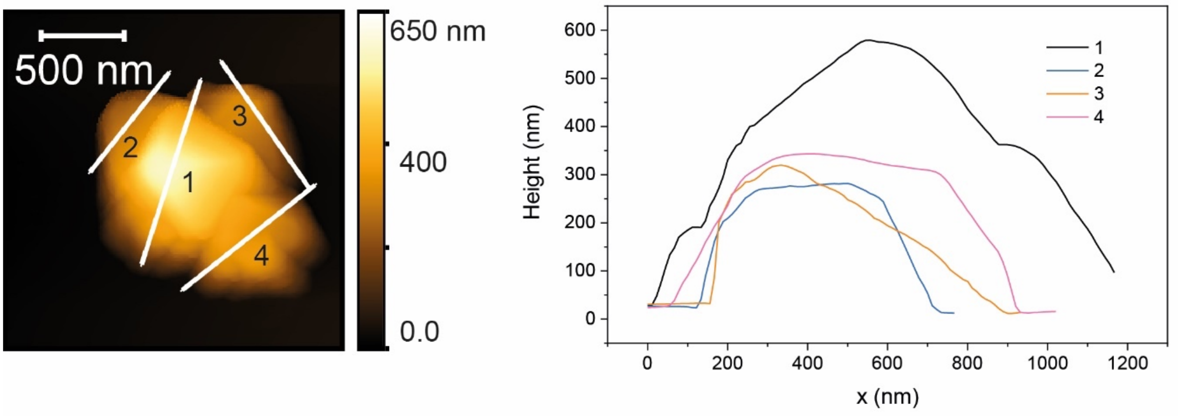

Figure S6: Height profiles of the fluorescein@UiO-66 crystals.

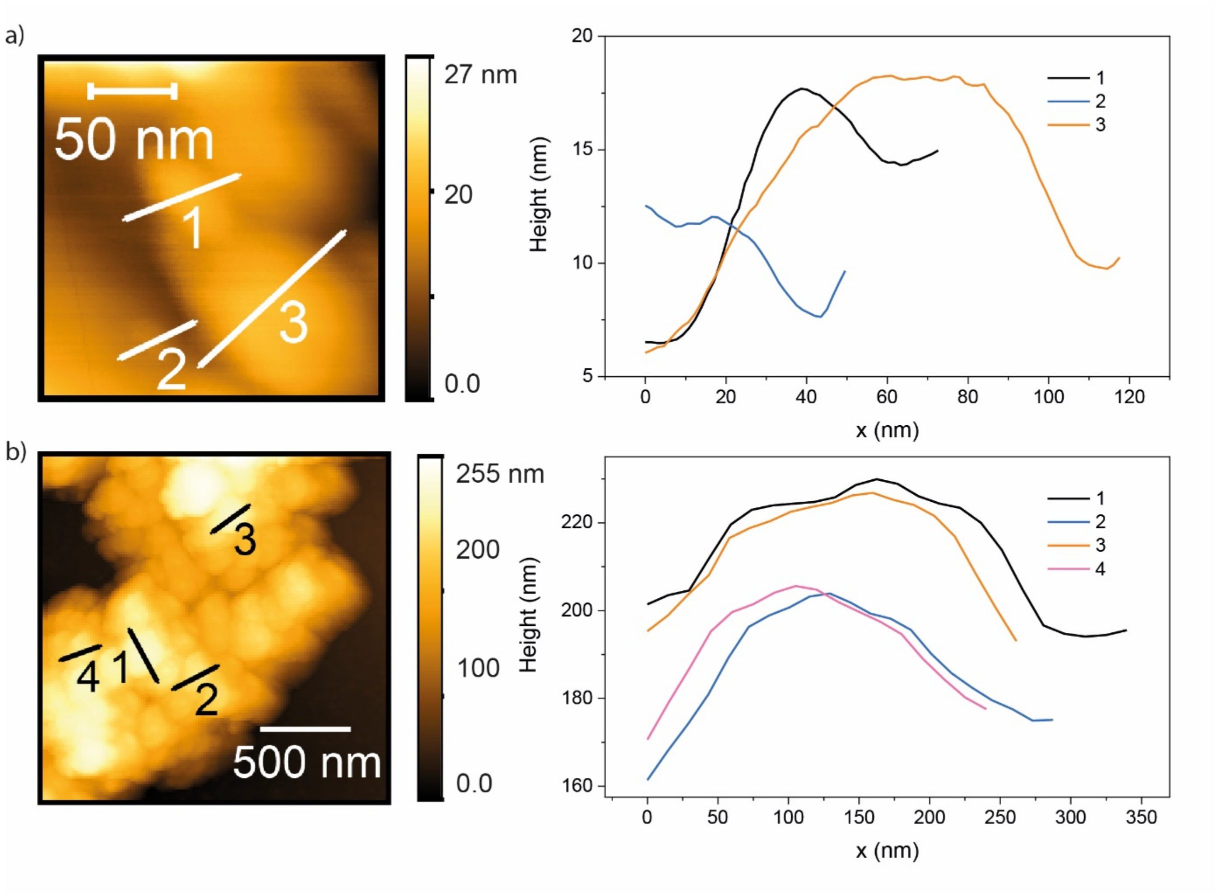

Figure S7: Height profiles of RhB@ZIF-8 nanocrystals: (a) as-synthesised and (b) after thorough washing.

3.3 SEM IMAGING

Backscattered electron and secondary electron SEM images were obtained at 10 keV under high vacuum. SEM characterisation was not only performed to image the MOF-type crystals, but to further confirm the absence of any residual guest material on the sample surface. The representative images of the samples at various locations are shown in Figures S8 and S9.

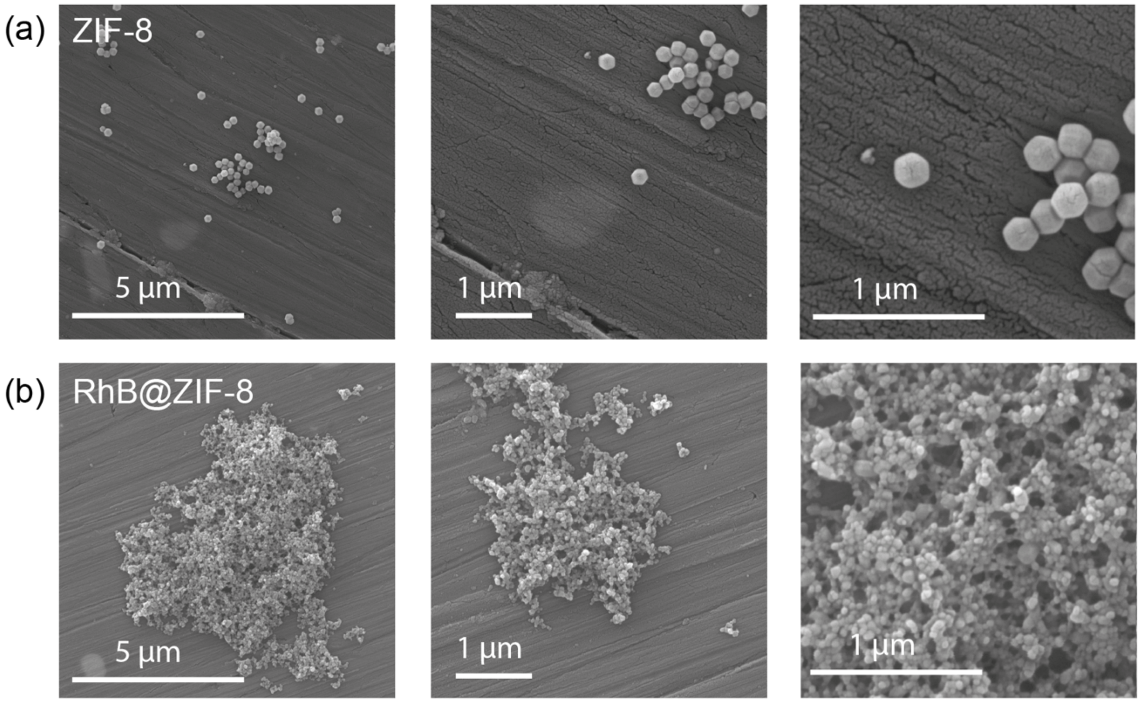

Figure S8: SEM micrographs of pristine (a) ZIF-8 and (b) RhB@ZIF-8 crystals.

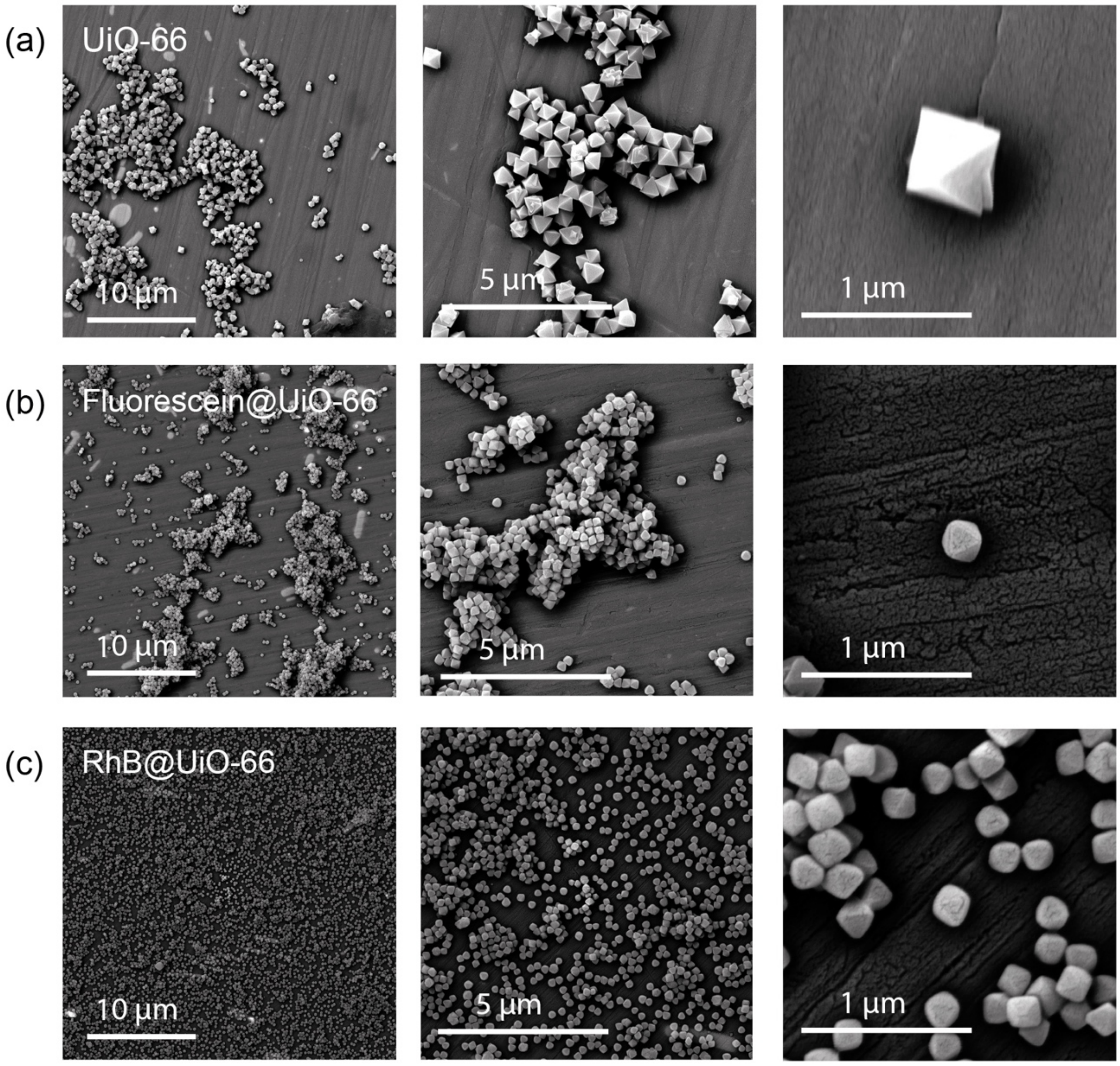

Figure S9: Backscattered electron SEM micrographs of the single crystals of (a) UiO-66, (b) fluorescein@UiO-66, and (c) RhB@UiO-66.

3.4 FLUORESCENCE LIFETIME IMAGING MICROSCOPY (FLIM)

Figure S10 shows that the lifetime of the fluorescein@UiO-66 single crystals is a monoexponential decay of 3.77 ns, which correlates well the lifetime observed for fluorescein in different solvents. Fluorescence lifetime images of three different crystals of UiO-66 are shown in Figure S11.

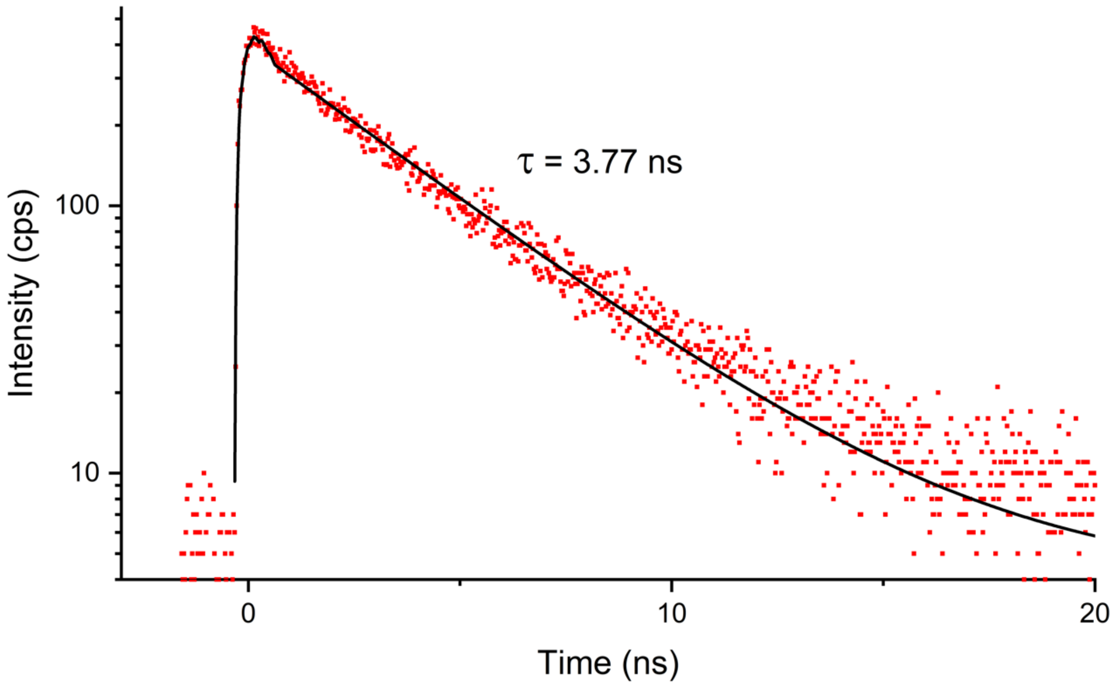

Figure S10: Average luminescence decay (lifetime) curve of several fluorescein@UiO-66 single crystals with mean lifetime of 3.77 ns (standard deviation: 0.15).

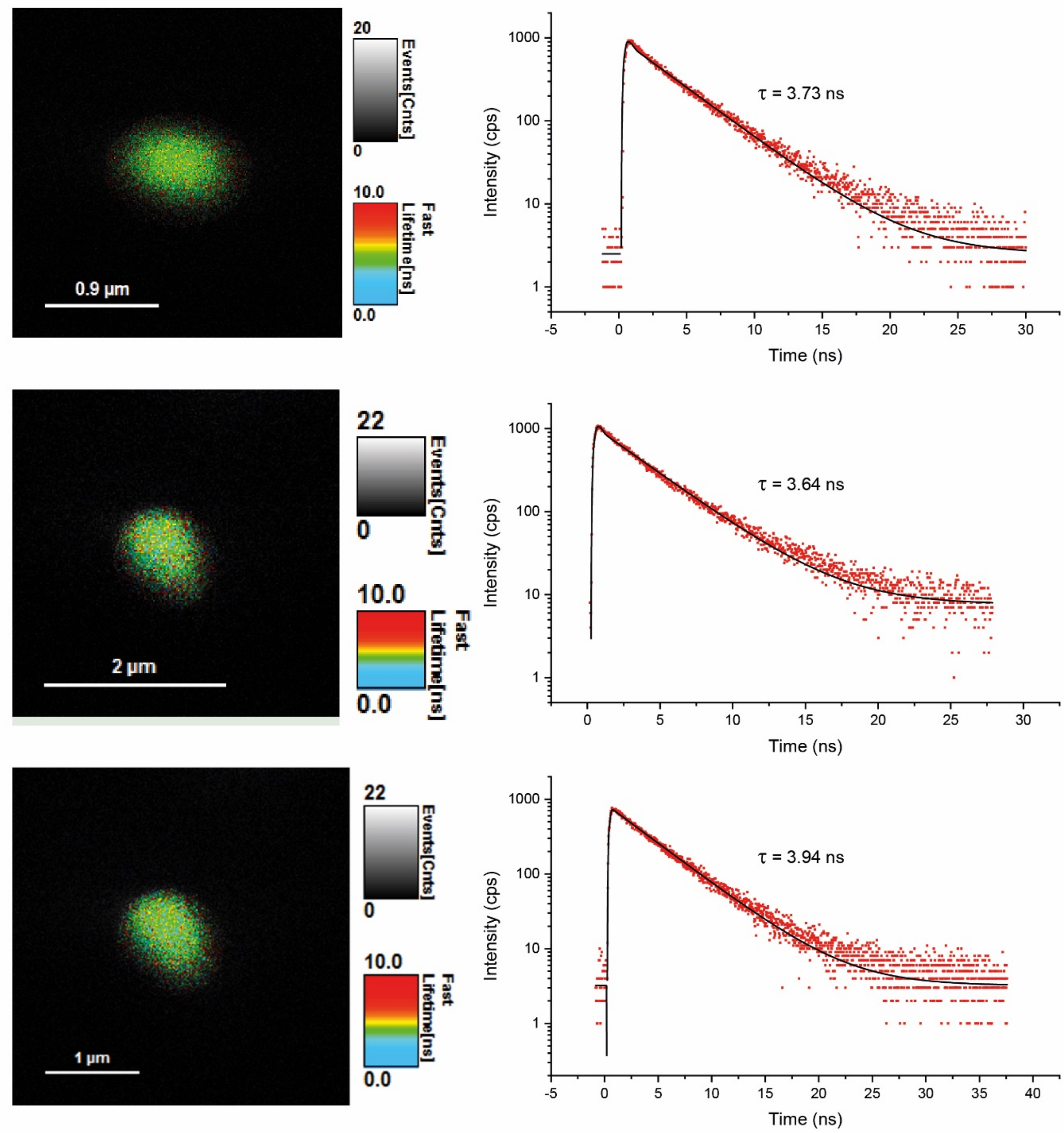

Figure S11: Fluorescence lifetime images and decay curves of fluorescein@UiO-66 single crystals (false colour scale).

3.5 WASHING PROCESS

The effectiveness of thorough washing has been confirmed by probing the supernatant of the last washing step. If any trace of the luminescent dye is still detectable, then the washing process has not been completed. However, due to the absence of any guest material found in the supernatant, we can conclude that the previous washing was thorough enough to remove any guest material. This is demonstrated by the absorption spectra of the supernatant – DMF in the case of Guest@UiO-66 and acetone for RhB@ZIF-8 – which show no signal of the guest (Fig. S12 a,c). In addition, emission spectra, with their higher sensitivity to the dyes, were measured and compared with the obtained Guest@MOF material (Fig. S12 b,d). Again, we found no sign of any guest material in the supernatant.

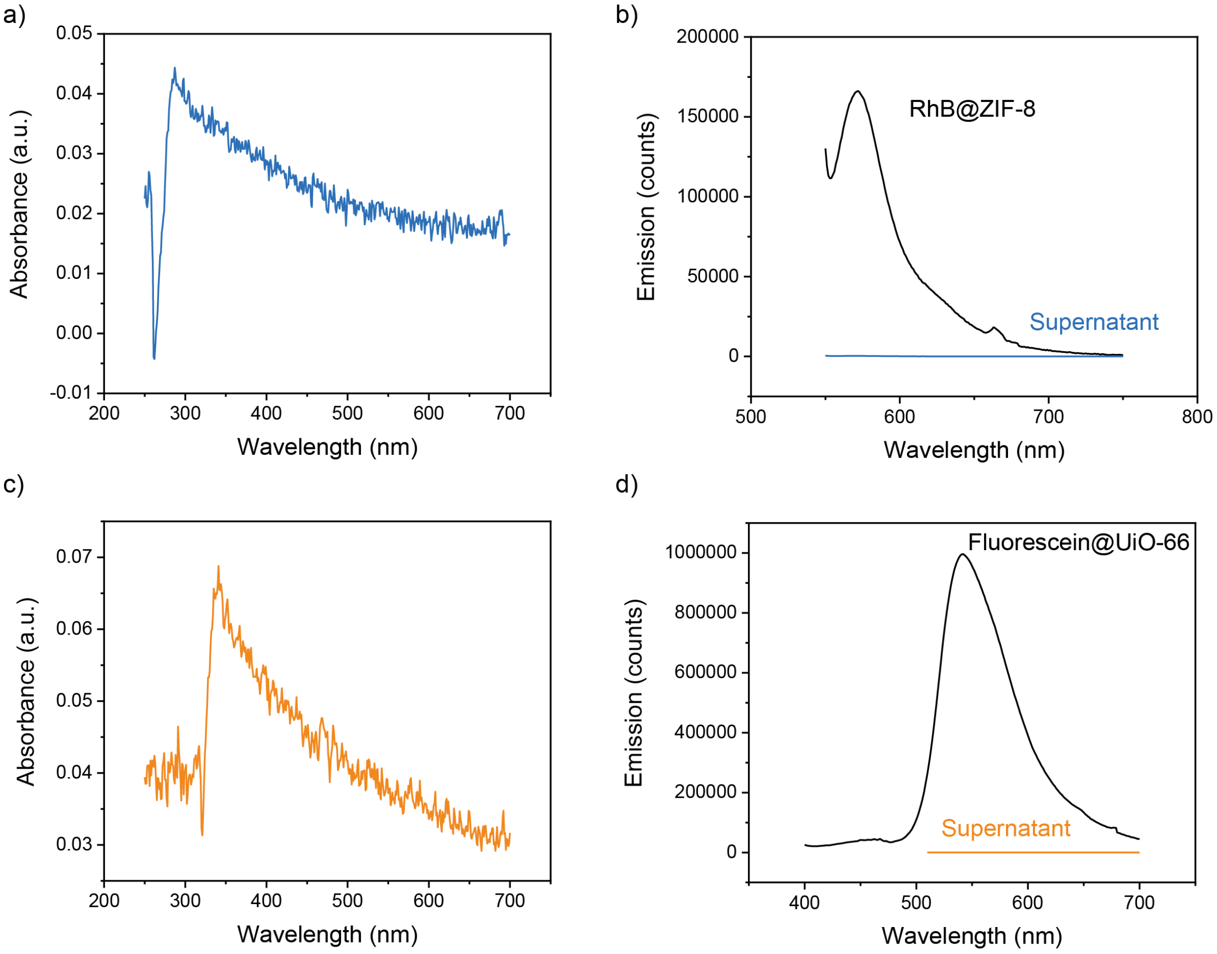

Figure S12: Absence of the dyes in the supernatant of the last washing step confirming thorough washing. a) Absorbance spectrum of acetone supernatant after removal of RhB@ZIF-8 showing no signal of RhB. b) Emission spectrum of acetone supernatant compared with the RhB@ZIF-8 (excitation wavelength 540 nm). c) Absorbance spectrum of DMF supernatant after removal of fluorescein@UiO-66 showing no signal of the fluorescein dye. d) Emission spectrum of DMF supernatant (excitation wavelength 500 nm) compared with the fluorescein@UiO-66 (excitation wavelength 380 nm).

4 REFERENCES

1. Su, Z.; Miao, Y.-R.; Zhang, G.; Miller, J. T.; Suslick, K. S. Bond breakage under pressure in a metal organic framework. *Chem. Sci.* **2017,** 8 (12), 8004-8011.
2. Keilmann, F.; Hillenbrand, R. Near-field microscopy by elastic light scattering from a tip. *Phil. Trans. R. Soc. A* **2004,** 362 (1817), 787-805.
3. Perdew, J. P.; Burke, K.; Ernzerhof, M. Generalized Gradient Approximation Made Simple. *Phys. Rev. Lett.* **1996,** 77 (18), 3865-3868.
4. Grimme, S. Semiempirical GGA-type density functional constructed with a long-range dispersion correction. *J. Comput. Chem.* **2006,** 27 (15), 1787-1799.
5. Dovesi, R.; Orlando, R.; Erba, A.; Zicovich-Wilson, C. M.; Civalleri, B.; Casassa, S.; Maschio, L.; Ferrabone, M.; De La Pierre, M.; D' Arco, P.; Noël, Y.; Causà, M.; Rérat, M.; Kirtman, B. CRYSTAL14 : A program for the ab initio investigation of crystalline solids. *Int. J. Quantum Chem.* **2014,** 114 (19), 1287-1317.
6. Noel, Y.; Zicovich-Wilson, C. M.; Civalleri, B.; D'Arco, P.; Dovesi, R. Polarization properties of ZnO and BeO: An ab initio study through the Berry phase and Wannier functions approaches. *Phys. Rev. B* **2001,** 65 (1), 014111.
7. Frisch, M. J., et al. *Gaussian 09, Revision A.02,* , Gaussian, Inc.: Wallingford CT, 2009.
8. Govyadinov, A. A.; Amenabar, I.; Huth, F.; Carney, P. S.; Hillenbrand, R. Quantitative Measurement of Local Infrared Absorption and Dielectric Function with Tip-Enhanced Near-Field Microscopy. *J. Phys. Chem. Lett.* **2013,** 4 (9), 1526-1531.
9. Chalmers, J. M.; Griffith, P. R., *Handbook of Vibrational Spectroscopy*. John Wiley & Sons, Ltd: 2006; Vol. 1.